www.springer.com/41230
https://doi.org/10.1007/s41230-022-1206-z

Microstructure characteristics and mechanical properties of $NbMoTiVWSi_x$ refractory high-entropy alloys

***Qin Xu[1], **Qi Wang[2], De-zhi Chen[2], Yi-ang Fu[1], Qing-sheng Shi[1], Ya-jun Yin[3], and Shu-yan Zhang[4]**

1. School of Mechanic and Electrical Engineering, Henan University of Technology, Zhengzhou 450001, China

2. National Key Laboratory for Precision Hot Processing of Metals, Harbin Institute of Technology, Harbin 150001, China

3. State Key Laboratory of Materials Processing and Die & Mould Technology, Huazhong University of Science & Technology, Wuhan 430074, China

4. Centre of Excellence for Advanced Materials, Songshan Lake, Dongguan 523808, Guangdong, China

***Qin Xu**

Ph.D, Associated Professor and Master Supervisor, Vice Director of Department of Materials Forming and Controlling Engineering in Henan University of technology. She mainly engages in advanced material solidification theory and casting technology, including titanium aluminum alloys, niobium silicon alloys, and high entropy alloys. To date, she has published more than 60 technical papers and a book, authorized 8 patents of invention.

E-mail: xuqin@haut.edu.cn

****Qi Wang**

Born in 1987, Ph.D, Lecturer. His research interests mainly focus on the melting and solidification process of titanium-based alloys and Nb-Si based ultrahigh temperature alloys.

E-mail: wangqi_hit@hit.edu.cn

Received: 2022-02-15
Accepted: 2022-07-24

Abstract: Refractory high-entropy alloys are considered as potential structural materials for elevated temperature applications. To obtain refractory high-entropy alloys with high strength, different amounts of Si were added into the NbMoTiVW refractory high-entropy alloys. The effects of Si on the phase constitution, microstructure characteristics and mechanical properties of $NbMoTiVWSi_x$ alloys were investigated. Results show that when the addition of Si is 0, 0.025 and 0.05 (molar ratio), the alloys are consisted of primary BCC and secondary BCC in the intergranular area. When the addition of Si is increased to 0.075 and 0.1, eutectic structure including silicide phase and secondary BCC phase is formed. The primary BCC phase shows dendritic morphology, and is refined by adding Si. The volume fraction of intergranular area is increased from 12.22% to 18.13% when the addition of Si increases from 0 to 0.1. The ultimate compressive strength of the NbMoTiVW alloy is improved from 2,242 MPa to 2,532 MPa. Its yield strength is also improved by the addition of Si, and the yield strength of $NbMoTiVWSi_{0.1}$ reaches maximum of 2,298 MPa. However, the fracture strain of the alloy is decreased from 15.31% to 12.02%. The fracture mechanism of the alloys is changed from mixed fracture of ductile and quasi-cleavage to cleavage fracture with increasing of Si. The strengthening of alloys is attributed to the refinement of primary BCC phase, volume fraction increment of secondary BCC phase, and formation of eutectic structure by addition of Si.

Keywords: high-entropy alloy; second phase; microstructure; refinement; mechanical property; strengthening

CLC numbers: TG146.4+16; Document code: A; Article ID: 1672-6421(2022)06-495-08

1 Introduction

Unlike traditional alloys, high-entropy alloys comprise multiple principal elements in equiatomic or near equiatomic concentrations rather than only a principal solvent element [1-6]. Among them, refractory high-entropy alloys normally consists of several principal refractory elements like W, Nb, Ta, Mo, Hf, Zr, etc., which usually form BCC solid solution phase during solidification process [7-12]. Refractory high-entropy alloys usually exhibit attractive mechanical properties at elevated temperature due to their high melting temperature and good solid solution strengthening effect. They are considered to be the most potential structural materials above 1,200 °C in the fields of ships, marine engineering, aerospace, and aviation [11-16].

Many series of refractory high-entropy alloys have been designed based on thermodynamics and dynamic theories, or computational techniques. Busch et al. [17] studied the solidification conditions of $Zr_{41.2}Ti_{13.8}Cu_{12.5}Ni_{10.0}Be_{22.5}$ alloy by analyzing the

Adam-Gibbs equation and found that solid solution is easy to form in the refractory high-entropy alloy with high viscosity. CALPHAD technique which can calculate phase diagram of alloys was also used to design refractory high-entropy alloys by predicting the phases of alloys [18-19]. Refractory high-entropy alloys, such as MoNbHfZrTi [8], MoNbTaTiV [20], NbTiVZr [21], ZrNbTiVHf [22], and HfNbTaTiZr [23], were reported by many researchers. Some research results also show that addition of Si, Al or rare metals can decrease the density and improve the properties of refractory high-entropy alloys [13, 24-31].

It is reported that addition of Si into refractory high-entropy alloys can change their phase constitutions, microstructures, and improve the mechanical properties. Guo et al. [28] reported that after adding Si, the phase constitutions of $NbTaWMoSi_x$ alloys change from single disordered BCC phase to multiphase of disordered BCC phase and silicide phase. Xu's study [24] shows that Si, addition into NbMoTiV can cause formation of BCC+M_5Si_3 eutectic at inter-dendrite areas, and the yield strength of $NbbMoTiVSi_{0.4}$ is improved up to 2,093 MPa. Liu's study [25] shows that multi-component silicide $(Hf, Nb, Ti)_5Si_3$ is generated after adding Si element into $HfMo_{0.5}NbTiV_{0.5}$, and exhibits a transition from hypoeutectic structure to eutectic structure and then to hypereutectic structure as Si content increases from 0 to 0.7. Furthermore, Si addition from 0 to 0.7 into $HfMo_{0.5}NbTiV_{0.5}Si_x$ alloys leads to an effective density reduction from 9.02 to 8.49 g·cm^{-3}, and yield strength of $HfMo_{0.5}NbTiV_{0.5}$ and $HfMo_{0.5}NbTiV_{0.5}Si_{0.7}$ alloys reaches 1,260 MPa and 2,134 MPa, respectively [25]. Guo's study [28] on $NbTaWMoSi_{0.25}$ alloy shows that the yield and ultimate strengthes at 1,200 °C reach 926 MPa and 1,071 MPa, respectively, while the fracture strain is only 13.11% [28].

Recently, studies on W-containing high-entropy alloys suggest that addition of W can improve the mechanical properties by solid solution strengthening effect [14, 32]. It also shows very good compatibility with element Nb, Mo, Ti, etc. Additionally, the binding effect between W and Si is much smaller than that between Nb, Mo, Ti, V and Si, indicating that W tends to distribute in BCC phase rather than in silicide. Thus, NbMoTiVW matrix alloy was prepared, and Si was selected to generate silicide during the melting process to improve the mechanical properties. In the present study, $NbMoTiVWSi_x$ (x=0, 0.025, 0.05, 0.075 and 0.1 in molar ratio) refractory high-entropy alloys were prepared by the non-consumable arc furnace, and the effects of Si on phase constitution, microstructure evolution and mechanical properties of $NbMoTiVWSi_x$ refractory high-entropy alloys were systematically investigated.

2 Experimental procedure

Refractory high-entropy alloys of $NbMoTiVWSi_x$ (x=0, 0.025, 0.05, 0.075 and 0.1 in molar ratio, hereinafter, named HW0, HW1, HW2, HW3 and HW4, respectively) were prepared by vacuum arc melting. The following high purity raw materials were used: sponge titanium (purity≥99.98%), vanadium blocks (purity≥99.98%), niobium sheets (purity≥99.98%), molybdenum blocks (purity≥99.98%), tungsten powders (purity≥99.98%), and silicon particles (purity≥99.98%). The physical properties of each element are shown in Table 1. The raw materials were weighed and put into a water-cooled copper crucible, then melted in an arc melting furnace with protection of high-purity argon. Button ingots with dimensions of about Φ60 mm×10 mm were obtained after melted five times in the crucible. Specimens with dimensions of 10 mm×10 mm×8 mm were cut from the obtained ingots for microstructure observation. X-ray diffraction (XRD, Panalytical Empyrean) with Cu Kα radiation was applied to determine phase constitutions of alloys with different additions of Si. The microstructure of ingots was observed by scanning electron microscopy (SEM, ZEISS EVO18) in back scattered-electron (BSE) mode. Compressive tests were done on an Instron 5569 Universal Tester with compression rate of 0.5 mm·min^{-1}. The dimensions of specimens for compression test was Φ4 mm×6 mm. Three specimens were measured for each ingot and the average was calculated as results. The fracture morphologies of alloys after compressive tests were observed by SEM (ZEISS Merlin Compact) in secondary electron (SE) mode.

Table 1: Physical properties of raw materials

Element	W	Mo	Nb	V	Ti	Si
Atomic number	74	42	41	23	22	14
Relative atomic mass (g·mol^{-1})	183.84	95.94	92.92	50.94	47.87	28.09
Melting temperature (°C)	3,410	2,610	2,468	1,890	1,670	1,410
Density (g·cm^{-3})	19.20	10.22	8.57	5.96	4.50	2.33
Atomic radius (Å)	1.367	1.363	1.429	1.316	1.462	1.153
Crystal structure	A2	A2	A2	A2	A3	A4
Electronegtivity	2.36	2.16	1.60	1.63	1.54	1.90
Valence electron concentration	6	6	5	5	4	4

3 Results

3.1 Phase analysis

Figure 1 shows XRD patterns of $NbMoTiVWSi_x$ refractory high-entropy alloys. It can be found that HW0 alloy without addition of Si consists of two BCC phase solid solutions, BCC1 and BCC2. The diffraction intensity of BCC1 is higher than that of BCC2, which indicates that BCC1 is the master phase in HW0 alloy. Peaks location of BCC2 implies that BCC2 phase is ordered in the present samples rather than the disordered one. The peaks at diffraction degree of about 40°, 58°, 73° and 87° are similar to those of the refractory elements W, Nb and Mo, which show higher diffraction intensity than that of Ti and V. When the addition of Si is 0.025, 0.5 and 0.075, the XRD patterns of HW1, HW2 and HW3 alloys are similar to that of HW0 alloy, showing that they are also consisted of BCC phase solid solution. When the addition of Si is 0.1, sharp increase of diffraction peaks at about 35° and 41° indicates the increase of BCC2 solid solution phase or formation of a new phase. According to microstructure observation by SEM, a new M_5Si_3 (M=Nb, Mo, Ti, V and W) phase is introduced, and the HW4 alloy consists of two BCC phase solid solutions and silicide M_5Si_3 phase. So, the HW4 alloy consists of two BCC phase solid solutions and silicide M_5Si_3 (M=Nb, Mo, Ti, V and W) phase. The diffraction peak intensity of M_5Si_3 phase is weaker than that of BCC1 phase, indicating that BCC1 phase is still the matrix phase in $NbMoTiVWSi_x$ alloys. Table 2 shows that the mixing enthalpy of Si with Mo, Nb, Ti, V and W are −35, −56, −66, −48 and −31 kJ·mol^{-1}, respectively. Their absolute values are all greater than that of the other element pairs. Therefore, Si tends to form intermetallics with other elements when its addition is relatively small. Thus, silicide phase will precipitate from the $NbMoTiVWSi_x$ alloys after adding different amounts of Si.

Moreover, the diffraction peaks of the master BCC1 phase for different alloys shift slightly to lower 2θ with increasing of Si (Table 3 and Fig. 2), indicating the increase of lattice parameters of BCC1 phase. As shown in Table 1, the difference between atomic radius of Nb, Mo, Ti, V, W is relatively small, and according to the Hume-Rothery rules, the smaller the atomic size difference, the easier to form substitutional solid solution of BCC phase. Silicon (Si) with smaller atomic radius of 1.153 Å is interstitial solid solution element. Therefore, addition of Si into $NbMoTiVWSi_x$ alloys may lead to formation of interstitial solid

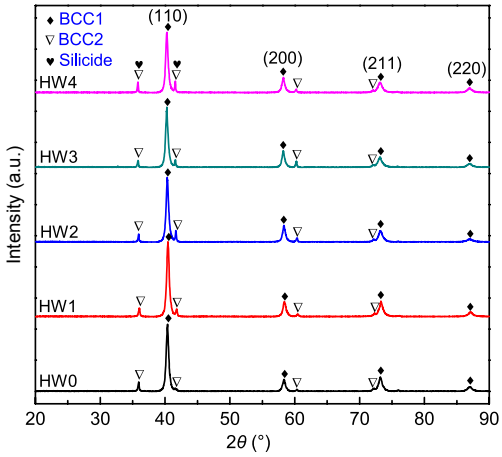

Fig. 1: XRD patterns for $NbMoTiVWSi_x$ alloys

Table 2: Mixing enthalpy (ΔH_{mix}, kJ·mol^{-1}) of different elements [34]

Element	Mo	Ti	V	W	Si
Nb	−6	2	−1	−8	−56
Mo		−4	0	0	−35
Ti			−2	−6	−66
V				−1	−48
W					−31

Table 3: 2θ for main peaks of $NbMoTiVWSi_x$ alloys

Alloy	Peak			
	(110)	(200)	(211)	(220)
HW0	40.447	58.434	72.379	87.215
HW1	40.394	58.408	72.273	87.112
HW2	40.393	58.381	72.223	87.086
HW3	40.263	58.252	72.196	87.059
HW4	40.289	58.252	72.089	87.031

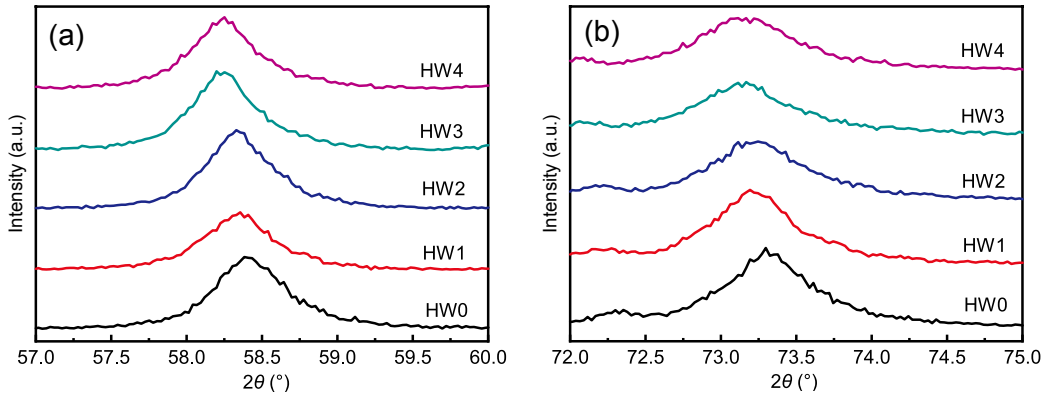

Fig. 2: Diffraction peaks of (200) (a) and (211) (b)

solution and cause lattice distortion of alloys. Consequently, certain addition amount of Si into $NbMoTiVWSi_x$ refractory high-entropy alloys shifts the peaks to lower 2θ direction.

The diffraction peaks of (200) and (211) for the $NbMoTiVWSi_x$ refractory high-entropy alloys are shown in Fig. 2. It can be seen that the diffraction peaks of (200) and (211) are not in perfect symmetry, which indicates that regular arrangement exists in some area of solid solution rather than random distribution. In other words, there exists element segregation in the $NbMoTiVWSi_x$ refractory high-entropy alloys. As is well known, the atoms with similar properties such as Mo and W exhibit selective-random distribution at high temperature, and therefore lead to elemental segregation in some area. On the other aspect, the mixing enthalpy of Mo with W is 0 $kJ \cdot mol^{-1}$, and the electronegativity of Mo and W is 2.16 and 2.36, respectively. Therefore, elements Mo and W can easily solute with each other, leading to element segregation.

3.2 Microstructure analysis

Figure 3 shows the microstructure of $NbMoTiVWSi_x$ refractory high-entropy alloys. Results show the primary BCC phase of alloys exhibit dendritic structure by adding different amounts of Si. The HW0 alloy without addition of Si show coarse dendrite morphology [Fig. 3(a)]. The white primary BCC dendrites show chrysanthemum morphology, and some black secondary phases with plate shape and tremella shape are formed in the intergranular area. According to the XRD results, both white primary phase and black phase are BCC solid solutions.

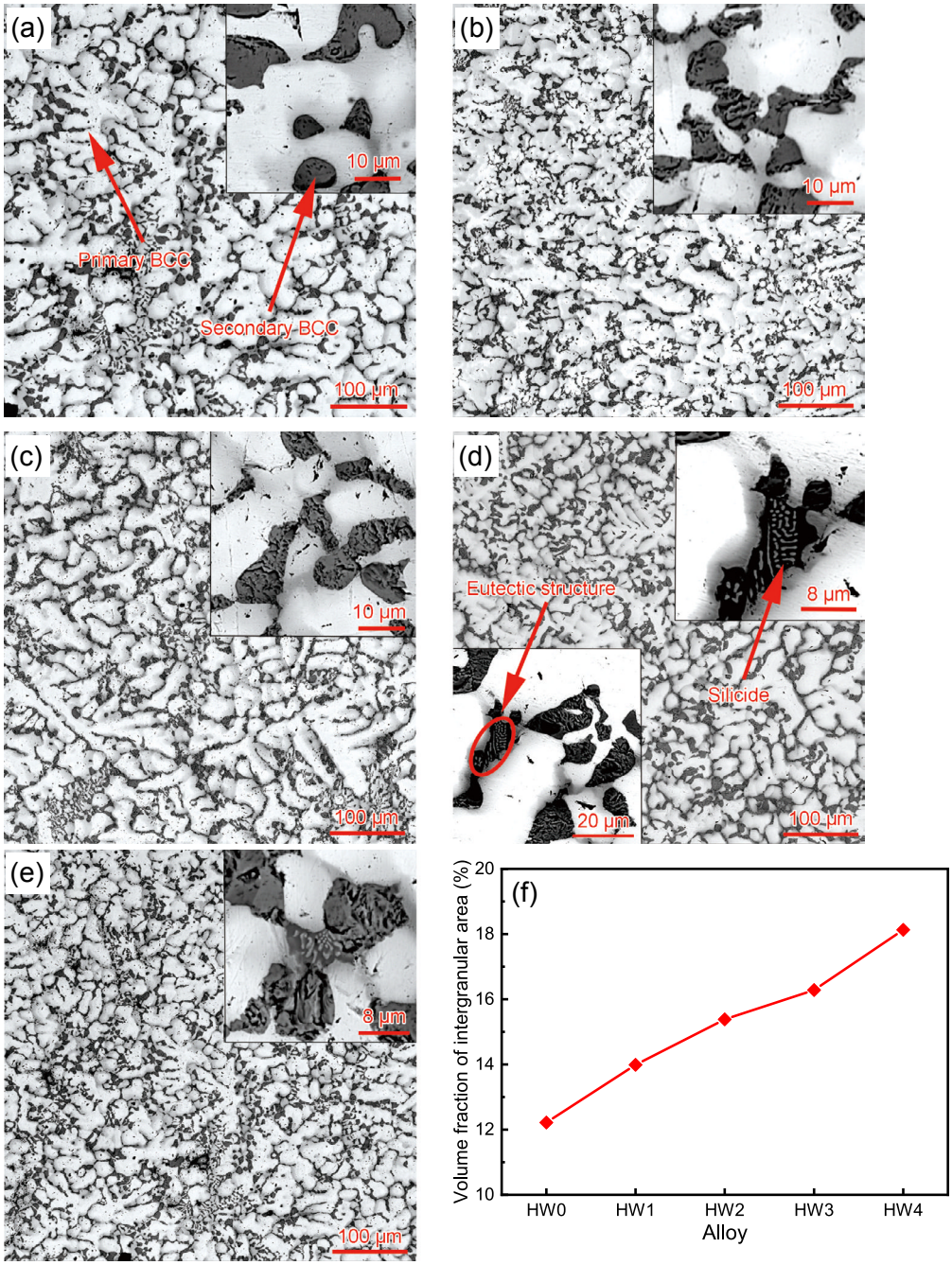

Fig. 3: Microstructure of $NbMoTiVWSi_x$ refractory high-entropy alloys: (a) HW0; (b) HW1; (c) HW2; (d) HW3; (e) HW4; (f) volume fraction of eutectic area

When addition of Si is 0.025 and 0.05 (molar ratio hereinafter), the primary BCC dendrites of HW1 and HW2 alloys are refined [Fig. 3(b) and Fig. 3(c)]. However, the morphology of primary BCC dendrites is not obviously changed, and they are still in a chrysanthemum shape. On the contrary, the morphology of secondary black BCC phase formed in the intergranular area is changed from mixture of smooth surface type and tremella shape to single tremella shape by addition of Si.

By adding 0.075 and 0.1 Si into HW0 alloy, the primary BCC phase of $NbMoTiVWSi_x$ alloys is still dendritic structure and is further refined [Fig. 3(d) and Fig. 3(e)]. Silicide phases with particle-like or rod-like shape are formed in the intergranular area of the alloys. Eutectic structure consisted of secondary BCC phase and silicide phase are also formed. The black secondary BCC phases are transformed into mixture of tremella shape and eutectic BCC phase by increasing of Si.

Figure 3(f) shows the volume fraction of intergranular area of $NbMoTiVWSi_x$ refractory high-entropy alloys. Volume fraction of intergranular area of HW0 alloy without addition of Si is about 12.22%, and it is increased by adding different amounts of Si. When addition of Si is 0.025 and 0.05, the intergranular areas of HW1 and HW2 alloys are BCC phase with tremella shape, and their volume fractions are 13.99% and 15.38%, respectively. When addition of Si is 0.075 and 0.1, the intergranular area of HW3 and HW4 alloys are BCC phase and eutectic structure, and their volume fractions are slightly increased to 16.28% and 18.13%, respectively.

EDS results of white primary BCC phase and intergranular area of $NbMoTiVWSi_x$ refractory high-entropy alloys are shown in Table 4. EDS results show that the primary white BCC phase of alloys is rich in W and Mo, while the intergranular area of alloys is rich in Nb and Ti. It reveals that elements W, Mo, Nb and Ti are seriously segregated in the alloys. W is an element with the highest melting temperature among the refractory metals, and it will be the first one to solidify during the solidification process of alloys. While the element, such as Ti, with lower melting temperature, usually has lower solubility in primary BCC phase. The Ti atoms will therefore be excluded from the primary BCC phase during the solidification process, and gathered in the residual melt. Consequently, element segregation will be formed after the whole melt is solidified.

3.3 Compressive properties

Compressive mechanical properties and morphology of fracture surface are shown in Figs. 4 and 5. It can be seen that the ultimate strength of alloys is improved from 2,185 MPa to 2,532 MPa by adding Si from 0 to 0.1, and yield strength is also improved from 2,136 MPa to 2,298 MPa. Both ultimate and yield strengths of HW4 alloy is the highest. However, fracture strain of alloys is reduced from 15.31% to 12.02% by addition of Si from 0 to 0.1. Therefore, addition of Si into HW0 alloy with molar ratio of 0.1 improves ultimate strength by 12.93%, and leads to the decrease of fracture strain by 21.48%. In a word, both ultimate and yield strength of alloys are improved by addition of Si, while fracture strain of alloys is decreased.

Figure 5 shows morphology of fracture surface of $NbMoTiVWSi_x$ refractory high-entropy alloys after compressive tests. Results show that the fracture surface of HW0 alloy without addition of Si exhibits some dimples, tearing

Table 4: EDS results of different phases in $NbMoTiVWSi_x$ refractory high-entropy alloys (at.%)

Alloy	Region	W	Mo	Nb	V	Ti	Si
	Nominal	20	20	20	20	20	–
HW0	White phase	56.18	18.78	11.51	7.88	5.65	–
	Black phase	11.70	5.36	37.67	5.58	39.70	–
	Nominal	24.84	24.84	24.84	24.84	24.84	0.64
HW1	White phase	66.59	14.29	8.26	6.65	4.21	–
	Eutectic structure	11.38	5.54	31.77	6.02	40.26	5.03
	Nominal	24.69	24.69	24.69	24.69	24.69	1.24
HW2	White phase	53.99	18.78	11.68	9.60	5.95	–
	Eutectic structure	9.79	5.15	34.44	5.50	39.69	5.43
	Nominal	24.54	24.54	24.54	24.54	24.54	1.84
HW3	White phase	56.01	18.23	10.75	9.33	5.68	–
	Eutectic structure	10.48	5.32	34.56	5.83	38.19	5.62
	Nominal	24.39	24.39	24.39	24.39	24.39	2.44
HW4	White phase	55.52	18.27	11.05	9.45	5.71	–
	Eutectic structure	12.22	5.38	34.63	5.21	36.77	5.79

ridges and river patterns [Fig. 5(a)], indicating that fracture mechanism of HW0 alloy is mixed fracture of ductile and quasi-cleavage fracture. HW1 alloy also shows mixed mode fracture of ductile and quasi-cleavage fracture, but with more tearing ridges and river-like patterns [Fig. 5(b)].

When Si addition reaches 0.05, though dimples disappear, tongue patterns and river patterns are found [Fig. 5(c)], the fracture mechanism of HW2 alloy is still mixed mode fracture of quasi-cleavage and ductile fracture. When Si addition reaches 0.075, HW3 alloy shows quasi-cleavage feature. Cleavage surfaces and river-like patterns appear on the fracture surface of HW3 alloy [Fig. 5(d)]. When Si addition reaches 0.1, in addition to the tongue patterns, cleavage steps appear. Thus, fracture mechanism of HW4 alloy is typical cleavage feature [Fig. 5(e)].

4 Discussion

4.1 Formation of silicide phase in alloys

Several parameters, such as mixing enthalpy, atomic radius difference, electronegativity difference and valence electron concentration have been proposed to predict phase formation in high-entropy alloys [2, 4, 35]. They can be used based on Hume-Rothery rule or from the thermodynamic point of view, and are ordinarily effective when the high-entropy alloys form simple solid solutions or intermetallic for high-entropy alloys. However, they cannot predict the type of intermetallics when elements can form more than one type of intermetallic in high entropy.

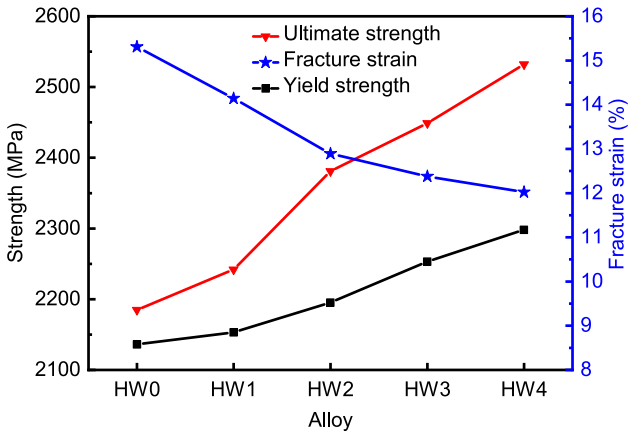

Fig. 4: Compressive mechanical properties of $NbMoTiVWSi_x$ refractory high-entropy alloys

As for $NbMoTiVWSi_x$ refractory high-entropy alloys in the present study, varies intermetallic silicides such as M_5Si_3, M_3Si, M_3Si_2, M_2Si, MSi_2 may be formed in the alloys according to the binary phase diagrams of Nb, Mo, Ti, V with Si. Actually, only M_5Si_3 silicide phase form in the $NbMoTiVWSi_x$ alloys when the addition of silicon is higher than 0.05, and the same phenomenon was also observed in many other refractory high-entropy alloys, such as $NbMoTiVSi_x$ [24, 27], $HfMo_{0.5}NbTiV_{0.5}Si_x$ [25], and $VNbTiTaSi_x$ [29] etc. From the binary phase diagrams of Nb, Mo, Ti, V with Si, it can be found that M_5Si_3-typed intermetallic phase can be formed for all metal elements in the $NbMoTiVWSi_x$ alloys, and the temperature to form M_5Si_3-typed phase is higher than that of other silicides. As for the sluggish diffusion effect of high-entropy alloys, the M_5Si_3-typed phase formed at high temperature can therefore be maintained to room temperature during the subsequent solidification process.

4.2 Microstructure refinement of alloys

Microstructure refinement is the most effective method to improve not only strength, but also ductility and fracture toughness by creating a more homogenous microstructure with more grain boundaries. It can be realized by (1) thermal method: increasing the supercooling degree of melting alloys; (2) chemical method: promoting nucleation and hindering growth by adding nucleating agents; or (3) mechanical method: vibration or agitation during the solidification process [36]. As for $NbMoTiVWSi_x$ refractory high-entropy alloys, the melting process and the solidification process are controlled identically to each other, microstructure is refined by different addition amounts of Si.

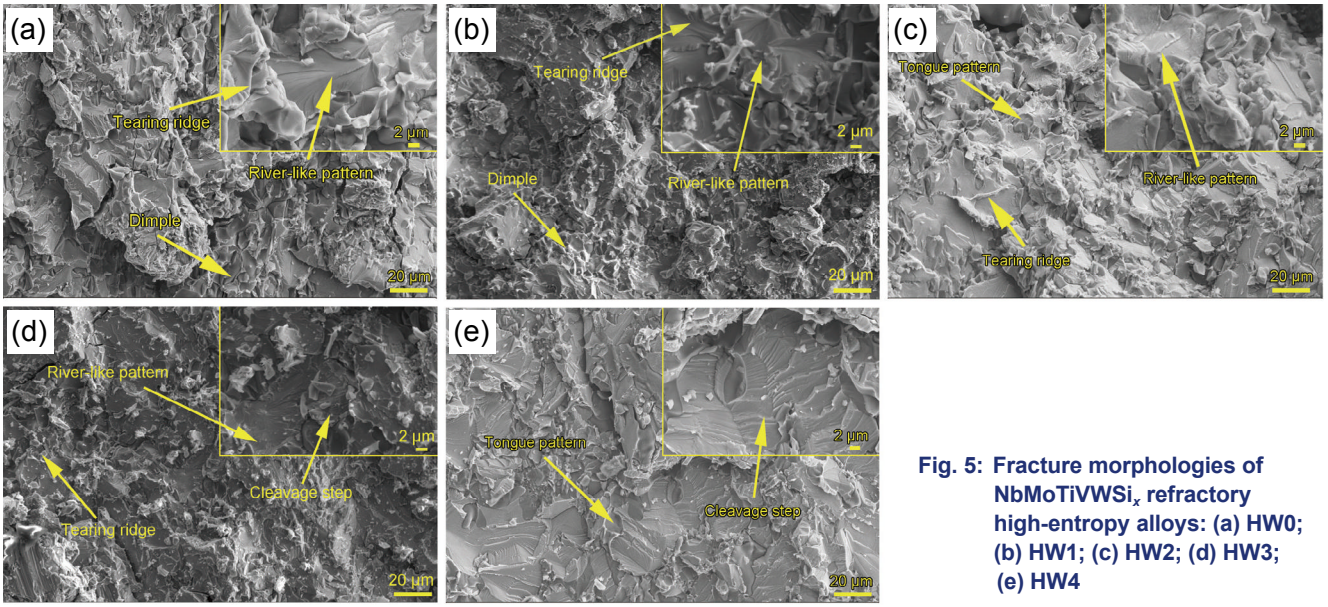

Fig. 5: Fracture morphologies of $NbMoTiVWSi_x$ refractory high-entropy alloys: (a) HW0; (b) HW1; (c) HW2; (d) HW3; (e) HW4

Addition of Si into NbMoTiVW high-entropy alloy can provide silicide particles as nuclei during solidification process. When temperature of the melt drops to lower than the liquidus of alloys, silicide particles first form in the liquid melt between silicon and elements with higher melting temperature (e.g. W, Mo). Then, the primary BCC solid solution phase heterogeneously nucleates based on the small silicide nuclei. The primary BCC phase continues to grow up and elements with lower melting temperature are propelled to the intergranular area. After that, the secondary BCC phase forms in the intergranular area when the addition of Si is 0.025 and 0.05, while eutectic reaction occurs and eutectic structure forms when the addition of silicon is 0.075 and 0.1. As a result, the alloys are refined by addition of Si.

4.3 Strengthening mechanism of alloys

Figure 6 shows the relationship between yield strength and volume fraction of intergranular area in $NbMoTiVWSi_x$ refractory high-entropy alloys. As shown in Fig. 6, when addition of Si is increased from 0 to 0.1, volume fraction of intergranular area is increased from 12.22% to 18.13%. In the meantime, yield strength is increased from 2,136 MPa to 2,298 MPa, respectively. The secondary BCC phase formed in the intergranular area acts as strengthening phase in $NbMoTiVWSi_x$ refractory high-entropy alloys. The increase of intergranular area is closely related to the increase of secondary BCC phase. Therefore, increase of secondary BCC phase can improve strength of $NbMoTiVWSi_x$ refractory high-entropy alloys owing to second phase strengthening. Additionally, the primary BCC phase is also refined by addition of Si, thus the refined primary BCC phase can also improve strength of $NbMoTiVWSi_x$ refractory high-entropy alloys owing to grain boundary strengthening.

Addition of Si into alloys can lead to formation of silicide phase or eutectic structure in the alloys [24-25, 37]. As has been reported, the formation of eutectic structure in alloys can cause strength improvement of high-entropy alloys [38-39]. Thus, eutectic structure formed in $NbMoTiVWSi_x$ refractory high-entropy alloys plays a positive role in improving the strength of the alloys. Consequently, both amount increase of secondary BCC phase and formation of eutectic structure by addition of Si

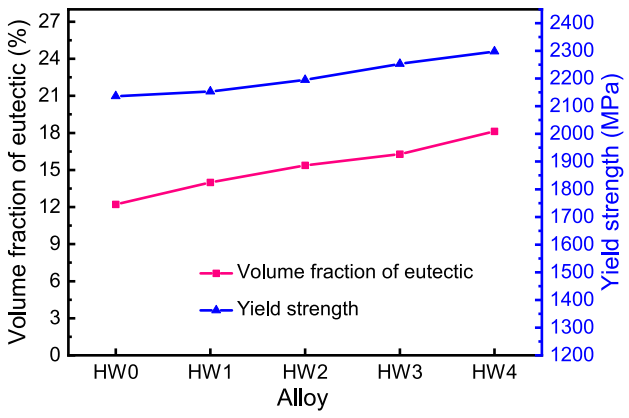

Fig. 6: Volume fraction of eutectic and yield strength of $NbMoTiVWSi_x$ refractory high-entropy alloys

improve the strength of $NbMoTiVWSi_x$ high-entropy alloys. Furthermore, addition of Si also leads to grain refinement of the primary BCC solid solution. Grain refinement strengthening is the main strengthening mechanism in most alloys [40-41]. Therefore, grain refinement by addition of Si can also improve the strength of $NbMoTiVWSi_x$ high-entropy alloys.

5 Conclusions

(1) Secondary BCC phase is formed in the intergranular area of $NbMoTiVWSi_x$ refractory high-entropy alloys, and the volume fraction of intergranular area is increased from 12.22% to 18.13% when the addition of Si is increased from 0 to 0.1.

(2) Element W with the highest melting temperature firstly solidifies from the melt during solidification process and therefore primary BCC phase with dendritic morphology is rich in W.

(3) Ultimate strength of alloys is increased from 2,242 MPa to 2,532 MPa, yield strength is increased from 2,136 MPa to 2,298 MPa, while fracture strain is decreased from 15.31% to 12.02% by increasing Si from 0 to 0.1.

(4) Improvement of the strength is owing to the refinement of primary BCC phase, volume fraction increment of secondary BCC phase, and formation of eutectic structure by addition of Si.

Acknowledgements

This work was financially supported by the National Natural Science Foundation of China (Grant Nos. 52001114, 51825401), Cultivation Program for Outstanding Young Teacher in Henan Province (Grant Nos. 21420152, 2021GGJS064), Scientific Research Fund of State Key Laboratory of Materials Processing and Die & Mould Technology (Grant No. P2020-023), Program for Guangdong Introducing Innovative and Entrepreneurial Teams (Grant No. 2016ZT06G025), and the Project of Science and Technology in Henan Province (Grant No. 192102210011).

References

[1] Cantor B, Chang I T H, Knight P, et al. Microstructural development in equiatomic multicomponent alloys. Materials Science and Engineering A, 2004, 375: 213–218.
[2] Yeh J W, Chen S K, Lin S J, et al. Nanostructured high-entropy alloys with multiple principal elements: Novel alloy design concepts and outcomes. Advanced Engineering Materials, 2004, 6(5): 299–303.
[3] Aitken Z H, Zhang Y W. Revealing the deformation twinning nucleation mechanism of BCC HEAs. MRS Communications, 2019: 1–7.
[4] Tsai K Y, Tsai M H, Yeh J W. Sluggish diffusion in Co-Cr-Fe-Mn-Ni high-entropy alloys. Acta Materialia, 2013, 61(13): 4887–4897.
[5] Gao N, Lu D H, Zhao Y Y, et al. Strengthening of a CrMnFeCoNi high-entropy alloy by carbide precipitation. Journal of Alloys and Compounds, 2019, 792: 1028–1035.
[6] Otto F, Dlouhý A, Somsen C, et al. The influences of temperature and microstructure on the tensile properties of a CoCrFeMnNi high-entropy alloy. Acta Materialia, 2013, 61(15): 5743–5755.

[7] Liu Q, Wang G F, Liu Y K, et al. Hot deformation behaviors of an ultrafine-grained MoNbTaTiV refractory high-entropy alloy fabricated by powder metallurgy. Materials Science and Engineering A, 2021, 809: 140922.
[8] Guo N N, Wang L, Su Y Q, et al. Microstructure and properties of novel quinary multi-principal element alloys with refractory elements. China Foundry, 2015(5): 319–325.
[9] Senkov O N, Wilks G B, Scott J M, et al. Mechanical properties of $Nb_{25}Mo_{25}Ta_{25}W_{25}$ and $V_{20}Nb_{20}Mo_{20}Ta_{20}W_{20}$ refractory high entropy alloys. Intermetallics, 2011, 19(5): 698–706.
[10] Mcalpine S W, Logan J V, Short M P. Predicting single phase stability and segregation in the NbMoTaTi-(W,V) high entropy alloy system with the vacancy exchange potential. Scripta Materialia, 2021, 191: 29–33.
[11] Cui H B, Wang Y, Wang J Y, et al. Microstructural evolution and corrosion behavior of directionally solidified FeCoNiCrAl high entropy alloy. China Foundry, 2011, 8(3): 259–263.
[12] Lo K C, Murakami H, Yeh J W, et al. Oxidation behaviour of a novel refractory high entropy alloy at elevated temperatures. Intermetallics, 2020, 119: 106711.
[13] Guo Y L, He J Y, Lu W J, et al. The evolution of compositional and microstructural heterogeneities in a $TaMo_{0.5}ZrTi_{1.5}Al_{0.1}Si_{0.2}$ high entropy alloy. Materials Characterization, 2021, 172: 110836.
[14] Coury F G, Kaufman M, Clarke A J. Solid-solution strengthening in refractory high entropy alloys. Acta Materialia, 2019, 175: 66–81.
[15] Senkov O N, Miracle D B, Chaput K J, et al. Development and exploration of refractory high entropy alloys – A review. Journal of Materials Research, 2018, 33(19): 3092–3128.
[16] Tian F Y, Wang D P, Shen J, et al. An ab initio investigation of ideal tensile and shear strength of TiVNbMo high-entropy alloy. Materials Letter, 2016, 166: 271–275.
[17] Busch R, Schroers J, Wang W H. Thermodynamics and kinetics of bulk metallic glass. MRS Bulletin, 2007, 32(8): 620–623.
[18] Miracle D, Miller J D, Senkov O, et al. Exploration and development of high entropy alloys for structural applications. Entropy, 2014, 16: 494–525.
[19] Senkov O N, Miller J D, Miracle D B, et al. Accelerated exploration of multi-principal element alloys with solid solution phases. Nature Communications, 2015, 6: 6529.
[20] Liu Q, Wang G F, Sui X C, et al. Microstructure and mechanical properties of ultra-fine grained MoNbTaTiV refractory high-entropy alloy fabricated by spark plasma sintering. Journal of Materials Science & Technology, 2019, 35(11): 2600–2607.
[21] Liao M Q, Liu Y, Min L J, et al. Alloying effect on phase stability, elastic and thermodynamic properties of Nb-Ti-V-Zr high entropy alloy. Intermetallics, 2018, 101: 152–164.
[22] Feuerbacher M, Lienig T, Thomas C. A single-phase bcc high-entropy alloy in the refractory Zr-Nb-Ti-V-Hf system. Scripta Materialia, 2018, 152: 40–43.
[23] Laplanche G, Gadaud P, Perriere L, et al. Temperature dependence of elastic moduli in a refractory HfNbTaTiZr high-entropy alloy. Journal of Alloys and Compounds, 2019, 799: 538–545.
[24] Xu Q, Chen D Z, Tan C Y, et al. $NbMoTiVSi_x$ refractory high entropy alloys strengthened by forming BCC phase and silicide eutectic structure. Journal of Materials Science & Technology. 2021, 60: 1–7.
[25] Liu Y, Zhang Y, Zhang H, et al. Microstructure and mechanical properties of refractory $HfMo_{0.5}NbTiV_{0.5}Si_x$ high-entropy composite. Journal of Alloys and Compounds, 2016, 694: 869–876.
[26] Schellert S, Gorr B, Laube S, et al. Oxidation mechanism of refractory high entropy alloys Ta-Mo-Cr-Ti-Al with varying Ta content. Corrosion Science, 2021, 192: 109861.
[27] Xu Q, Chen D Z, Wang C R, et al. Effect of Lanthanum on microstructure and mechanical properties of $NbMoTiVSi_{0.2}$ refractory high entropy alloys. Transactions of Nonferrous Metals Society of China, 2021, 31(2): 512–520.
[28] Guo Z M, Zhang A J, Han J S, et al. Effect of Si additions on microstructure and mechanical properties of refractory NbTaWMo high-entropy alloys. Journal of Materials Science, 2019, 54: 5844–5851.
[29] Yang X M, An Z B, Zhai Y D, et al. Effect of Al content on the thermal oxidation behaviour of AlHfMoNbTi high-entropy alloys analysed by in situ environmental TEM. Corrosion Science, 2021, 191: 109711.
[30] Guo N N, Wang L, Luo L S, et al. Microstructure and mechanical properties of refractory high entropy $(Mo_{0.5}NbHf_{0.5}ZrTi)$ BCC/M_5Si_3 in-situ compound. Journal of Alloys and Compounds, 2016, 660: 197–203.
[31] Yao H W, Miao J W, Liu Y M, et al. Effect of Ti and Nb contents on microstructure and mechanical properties of $HfZrVTaMoWTi_xNb_y$ refractory high-entropy alloys. Advanced Engineering Materials, 2021, 23(8): 2100225.
[32] Raman L, Anupam A, Karthick G, et al. Strengthening mechanisms in CrMoNbTiW refractory high entropy alloy. Materials Science and Engineering A, 2021, 819: 141503.
[33] Li Q Y, Zhang H, Li D C, et al. WxNbMoTa refractory high-entropy alloys fabricated by laser cladding deposition. Materials, 2019, 12(3): 1–14.
[34] Takeuchi A, Inoue A. Classification of bulk metallic glasses by atomic size difference, heat of mixing and period of constituent elements and its application to characterization of the main alloying element. Materials Transactions, 2005, 46(12): 2817–2829.
[35] Zhang Y, Zuo T T, Tang Z, et al. Microstructures and properties of high-entropy alloys. Progress in Materials Science, 2014, 61: 1–93.
[36] Al-Qawabah S M A, Zaid A I O. Different methods for grain refinement of materials. International Journal of Scientific and Engineering Research, 2016, 7: 1133–1140.
[37] Xu Q, Fang H Z, Wu C, et al. Microstructure evolution and its effect on mechanical properties of cast Ti48Al6NbxSi alloys. China Foundry, 2020, 17(6): 416–422.
[38] Lu Y P, Gao X Z, Jiang L, et al. Directly cast bulk eutectic and near-eutectic high entropy alloys with balanced strength and ductility in a wide temperature range. Acta Materialia, 2017, 124: 143–150.
[39] Lu Y P, Dong Y, Guo S, et al. A promising new class of high-temperature alloys: Eutectic high-entropy alloys. Scientific Reports, 2014, 4: 6200.
[40] Shu D L, Xie J, Zhang F J, et al. Room temperature tensile deformation behavior of a Ni-based superalloy with high W content. China Foundry, 2021, 18(3): 192–198.
[41] Njuguna B K, Li J Y, Tan Y, et al. Grain refinement of primary silicon in hypereutectic Al-Si alloys by different P-containing compounds. China Foundry, 2021, 18(1): 37–44.